Neuroscience

Neural Geometry from Mixed Sensorimotor Selectivity for Predictive Sensorimotor Control

Reviewed Preprint
v1 • August 7, 2024
Not revised

Yiheng Zhang, Yun Chen, Tianwei Wang, He Cui

Center for Excellence in Brain Science and Intelligence Technology, Institute of Neuroscience, Chinese Academy of Sciences, Shanghai 200031, China • Chinese Institute for Brain Research, Beijing, 102206, China • University of Chinese Academy of Sciences, Beijing 100049, China

Abstract

Summary

Although recent studies suggest that activity in the motor cortex, in addition to generating motor outputs, receives substantial information regarding sensory inputs, it is unclear how sensory context adjusts the motor commands. Here, we recorded population neural activity in the motor cortex via microelectrode arrays while monkeys performed flexible manual interceptions of moving targets. During this task, which requires predictive sensorimotor control, the activity of most neurons in the motor cortex encoding upcoming movements, was influenced by ongoing target motion. Single-trial neural states at movement onset formed staggered orbital geometries, suggesting that target speed modulates pre-movement activity in an orthogonal manner. This neural geometry was further evaluated with a representational model and a recurrent neural network (RNN) with task-specific input-output mapping. We propose that sensorimotor dynamics can be derived from neuronal mixed sensorimotor selectivity and dynamic interaction between modulations.

eLife assessment

This **useful** study examines the neural activity in the motor cortex as a monkey reaches to intercept moving targets, focusing on how tuned single neurons contribute to an interesting overall population geometry. The presented results and analyses are **solid**, though the investigation of this novel task could be strengthened by clarifying the assumptions behind the single neuron analyses, and further analyses of the neural population activity and its relation to different features of behaviour.

https://doi.org/10.7554/eLife.100064.1.sa4

Introduction

The motor cortex, a brain region generating motor commands, is widely known for its relation to movement kinetics[1,2] and kinematics[3–5]. Moreover, it has been reported to also carry substantial sensory information[6–13]. Activity in the motor cortex can be strongly influenced by reference frame[14], hand trajectory[15], and stimuli for target selection[16]; there even exists evoked activity during visual replay related to the tracking movements[17]. However, it is unclear how such sensory input contributes to pre-movement activity in the motor cortex.

From the dynamical systems perspective, preparatory population activity develops toward a movement-specific optimal subspace to set initial states seeding the motor generation[18–20]. However, sensory information may change the distribution of neural states during movement in an orthogonal fashion without affecting the motor output.

To investigate the neural dynamics shaped by concurrent sensorimotor signals, we recorded population activity in the primary motor cortex (M1) from monkeys performing a flexible manual interception task. Unlike previous studies constraining interception at a fixed location[9,21], our task demands predictive spatiotemporal mappings to displace a body effector to a trial-varying location. We found that the activity of most neurons was jointly tuned to both reach direction and target motion via directional selectivity shifts, gain modulations, offset adjustments, or their combinations. Strikingly, such mixed sensorimotor selectivity exists throughout the entire trial, in contrast to the gradient of sensory-to-motor tuning from cue to movement epochs in posterior parietal cortex (PPC) that we recently reported [22,23]. Principal component analysis (PCA) of the neural population revealed a clear orbital neural geometry in low-dimensional space at movement onset: The neural states were distributed in reach-direction order, and formed ringlike structures whose slopes were determined by target-motion conditions. Neuronal simulation indicates that these characteristics of neural population dynamics could be derived from the mixed sensorimotor selectivity of single neurons. A recurrent neural network (RNN) trained with proper input-output mappings offers insights into the relationship between neuronal modulation and neural geometry in a dynamical system. We propose that this sensory modulation occurs at both single-neuron and population levels as a general element of neural computations for predictive sensorimotor control.

Results

Mixed tuning of M1 single neurons during flexible manual interception task

Three monkeys (*Macaca mulatta*, C, G, and D, male, weight 7 to 10 kg) were trained to perform a delayed manual interception task (**Figure 1A**), which was modified from that utilized in our recent studies [22,23]. To initiate a trial, the monkey needed to hold the center dot of a standing touch screen for 600 ms. Then, a peripheral target appeared, either stationary or rotating around the center dot at a constant angular speed. The monkey was required to wait during a random delay (400-800 ms) until the central dot went dark (GO) and then to immediately reach to the target. Once the monkey touched the screen (Touch), the target stopped and another dot showed the touching location, in red for a successful interception or in blue for a failure. The error tolerance between the target and the touch location (reach endpoint) was 3 cm. There were five targetmotion conditions, consisting of clockwise (CW) conditions - 240 °/s and -120 °/s, counterclockwise (CCW) conditions 120 °/s and 240 °/s, along with 0 °/s (static) condition. We define the target-speed magnitude as TS_{mag} (0 °/s, 120 °/s, and 240 °/s) and the target-speed direction as

TS_{dir} (CCW and CW). These target-motion conditions were interleaved trial by trial, and initial location of the target was random. The reach endpoints of a well-trained monkey distributed uniformly around the circle (**Figure 1B**, Rayleigh's test: p=0.36; data from monkey C, 772 correct trials in one session). Because the reach direction was defined as the angle of the reach endpoint, for simplicity, we divided the circular space equally into eight sectors (45° per each), and grouped trials according to the eight reach directions and five target-motion conditions.

We recorded neural data with Utah arrays from monkeys C, G, and D (implanted sites are shown in **Figure 1C**, and all datasets listed in Table S1) and hand trajectories from monkeys C and G (Figure S1), during the interception task. The hand trajectory was launched to the final interception position. The temporal profiles of hand velocity were unimodal bell-like curves and similar across target-motion conditions (correlation coefficients is 0.97±0.05 for monkey C and 0.99±0.02 for monkey G).

Notably, we found that neuronal directional tuning during motor execution (MO±100 ms, MO for movement onset) was modulated by target motion, according to our statistical criteria mainly in three ways: preferred direction (PD) shift, gain, and offset addition (**Figure 1D** and Figure S2-S4, Methods). PD-shift neurons had their PDs shifted in moving-target conditions compared to the static-target condition. As illustrated by an example neuron (**Figure 1D**, *PD shift*), whose PDs corresponding to CCW conditions (red and yellow) and CW conditions (blue and purple) exhibited obvious differences, TS_{dir} rather than TS_{mag} dominated this modulation. Gain-modulation neurons exhibited reach-direction tuning multiplied by target speed: while their directionality remained invariant, the neuronal responses at PD differed across target-motion conditions. This modulation was dominated by TS_{dir} as well. The turning curves of the example neuron (**Figure 1D**, *Gain*) had higher responses at PD in CW conditions (blue and purple) than in the others (green, yellow, and red), indicating a varying tuning depth for reach direction. Neurons with addition modulation underwent changes of offset activity induced by target speed (both TS_{dir} and TS_{mag}). As shown by the example neuron (**Figure 1D**, *Addition*), this effect was almost equal for all reach directions.

The activity of these example neurons could be well explained by PD shift, gain, and additive models (**Figure 1E**, *Methods*), respectively. Nevertheless, it was difficult to classify all neurons with mixed sensorimotor selectivity into one of these three groups exclusively, because many of them experienced a mixture of two or three of above modulations. Moreover, the proportions of three groups were almost equal (**Table 1**). We found that the adjusted R_2 of a full model (0.64 ± 0.21, mean ± sd.) was larger than that of the PD shift (0.59 ± 0.23), gain (0.56 ± 0.21), and additive (0.47 ± 0.24) models for monkey C (95 neurons), as well as for all three monkeys (rank-sum test, p<0.01, Figure S5). These target-motion modulations of neuronal directionality suggested the participation of sensory signals in shaping neural dynamics during interception execution.

Single neurons were classified by comparing firing rate patterns between target-speed conditions (more details in **Methods**). The first column is the mean±std. of recording unit number in one monkey across sessions. The other columns give the ratio of target-speed modulation unit across sessions.

Coding of sensory and motor information in neural populations

To quantify target motion information embodied in neural response in motor cortex, we performed a series of decoding analyses on the neural data from monkey C (n=95, 772 correct trials). To begin with, neural data were utilized to train a support vector machine (SVM) classifier for targetmotion conditions (one in five), and another for reach directions (one in eight; Methods).

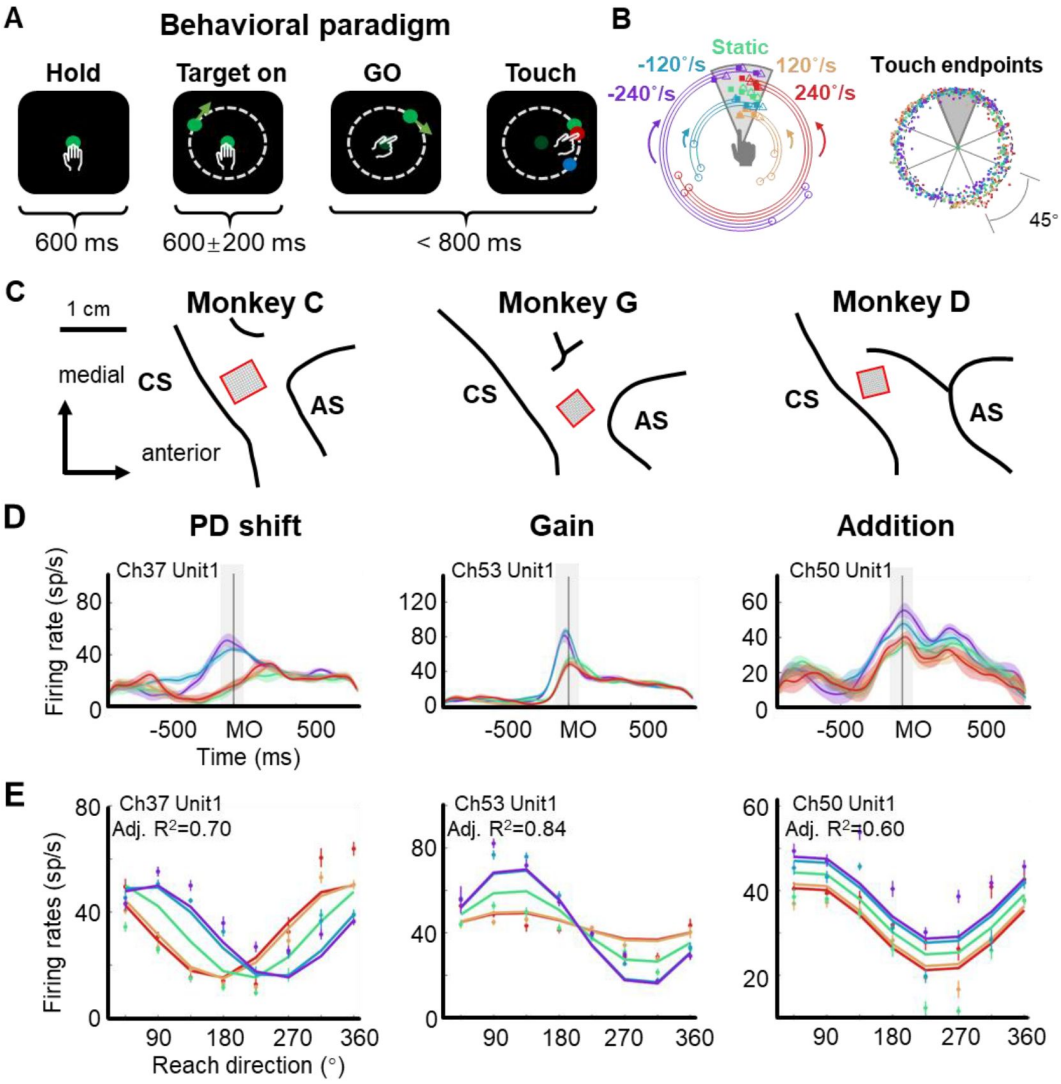

Figure 1.

Flexible manual interception task and behavioral performance

A Diagram of interception task.
B Touch endpoints distribution. Left panel shows three reaching-up example trials in five targetmotion conditions. The squares label the touch endpoints, and the circles and triangles are the target onset and stop location. The five target-motion conditions (-240°/s, - 120°/s, 0°/s, 120°/s, and 240°/s) are indicated in five colors (purple, blue, green, yellow, and red). Target starting location is randomly distributed. Right panel shows that the touch endpoints had uniform distribution around the circle (monkey C 772 trials, Rayleigh's test, p=0.36).
C Implanted locations of microelectrode array in the motor cortex of the three well-trained monkeys. Neural data were recorded from the cortical regions contralateral to the used hand. AS, arcuate sulcus; CS, central sulcus.
D Three example neurons with PD shift, gain modulation, and offset addition. The peri-stimulus time histograms (PSTH) show the activity of example neurons when monkeys reached to upper areas in five target-motion conditions.
E The directional tuning curve of three example neurons with PD shift, gain, and addition modulation around movement onset (MO ± 100 ms, the same neurons as in **Figure 1D**, adjusted R_2 of three neurons: 0.70, 0.84, and 0.60). Dots and bars denote the average and standard error of firing rates, respectively, colored as target-motion conditions.

Proportion of various modulation neurons	Gain (G)	PD shift (S)	Addition (A)	None
Monkey C N=84.9±15.9, 7 sessions	46.9±15.9%	79.0±8.9%	61.9±14.5%	6.5±6.2%
Monkey G, N=97.5±17.7, 4 sessions	29.3±4.9%	51.6±29.1%	25.9±8.3%	25.5±15.8%
Monkey D, N=44.5±7.5, 4 sessions	45.6±13.8%	74.4±8.8%	49.1±9.1%	10.8±5.4%
RNN, N=200 100 models	30.5±3.5%	26.6±3.1%	37.9±6.6%	43.9±4.6%

Table 1.

Ratio of M1 neurons modulated by target speed around movement onset

As **Figure 2A** shows, the decoding accuracy of the target-motion condition increased quickly and peaked at over 70% around GO, while the decoding accuracy of reach direction climbed and reached a plateau of about 80% before MO. These results are similar to those of the other two monkeys and the pseudo-populations (Figure S6), suggesting that target motion information existed in M1 throughout almost the entire trial. According to the demixed PCA results, while reach direction occupied top components, there was interaction components that should not be neglected and even explained more variance than target speed components (Figure S7)[24].

Then, another decoding analysis was implemented to probe the potential interaction between reach-direction and target speed during execution period. We trained a reach-direction decoder (one in eight) to check if the decoder of one certain target-motion condition could be transferred to other conditions (**Figure 2B** left). It turned out that the performance of the transferred decoder deteriorated more significantly for $TS_{dir.}$ (CCW *vs*. CW, mean ± sd. of accuracy 0.26±0.06), compared with that for TS_{mag} (120 *vs*. 240, 0.50±0.06, paired t-test, $p<0.01$) and for target's state (static *vs*. motion 0.55±0.06, paired t-test, $p<0.01$). This result suggests that the coding of reach direction was rather sensitive to $TS_{dir,}$ but containing similarities for static and moving targets. As control, we also compared the neural coding rules across different reach-direction conditions. We trained a target-speed decoder (one in five), and similarly checked the transferred decoding accuracy (**Figure 2B** right). We observed that the target-speed decoder was locked with reach direction, as the transferred decoding accuracy diminished with increasing difference of reach direction. These results qualitatively imply the interaction as that target speeds affected the reach-directional tuning, especially by $TS_{dir.}$.

To explore how sensory information influences neural dynamics while preserving motor output, we performed PCA on the normalized population activity. We obtained the trial-averaged neural trajectories (5 target speeds x 8 reach directions 40 conditions) after TO or after GO (Figure S8A). The distance between neural trajectories grouped by reach-direction conditions was larger than the distance grouped by target-speed conditions especially after GO (Figure S8B), consistent with the demixed PCA results that M1 primarily encoded reach direction rather than target speed. In addition, the distance of neural trajectories between CCW and CW was much larger than the distance between 120°/s and 240 °/s conditions, indicating that TS_{dir} dominated the target-speed effect, agreeing with the decoding results (Figure S8C).

However, these neural trajectories were not yet the ideal description, because they were shaped mostly by time. So, to highlight the proposed target-speed effect on reach direction, we focused on four key time windows and snapshotted the neural trajectory as neural state to extract the coding rule at single trial level and in a geometric view. Here, we define the "neural states" as the projection of single-trial data during a specific time bin on principal components[25–27]. At MO, the first two principal components (PCs) of the neural states explained the most variance ([24.8%, 13.8%]) and were most related to reach direction (the goodness of fitting reach direction, $[R^2_{pc1}, R^2_{pc2}] = [0.82, 0.81]$, **Figure 2C**). While reach direction was represented by the first two PCs at GO and during movement execution, target speed influenced the tuning pattern of the first three PCs (**Figure 2D**), suggesting that target motion affects M1 neural dynamics via a topologically invariant transformation.

Orbital neural geometry in latent space

We visualized the neural states in the low-dimensional space spanned by the above three PCs at MO. The projections of the single-trial neural state onto the PC1-PC2 subspace clustered, or rather distributed, in reach-direction order (**Figure 3A** top and **Figure 3B** left). Interestingly, the neural states formed ringlike structures under single target-motion conditions and the fitted ellipses exhibited concentric shapes (the fitting goodness of ellipses, R_2 = 0.92 ± 0.01, mean ± sd., see Methods). Moreover, these ellipses tilted in condition-dependent angles, which is particularly

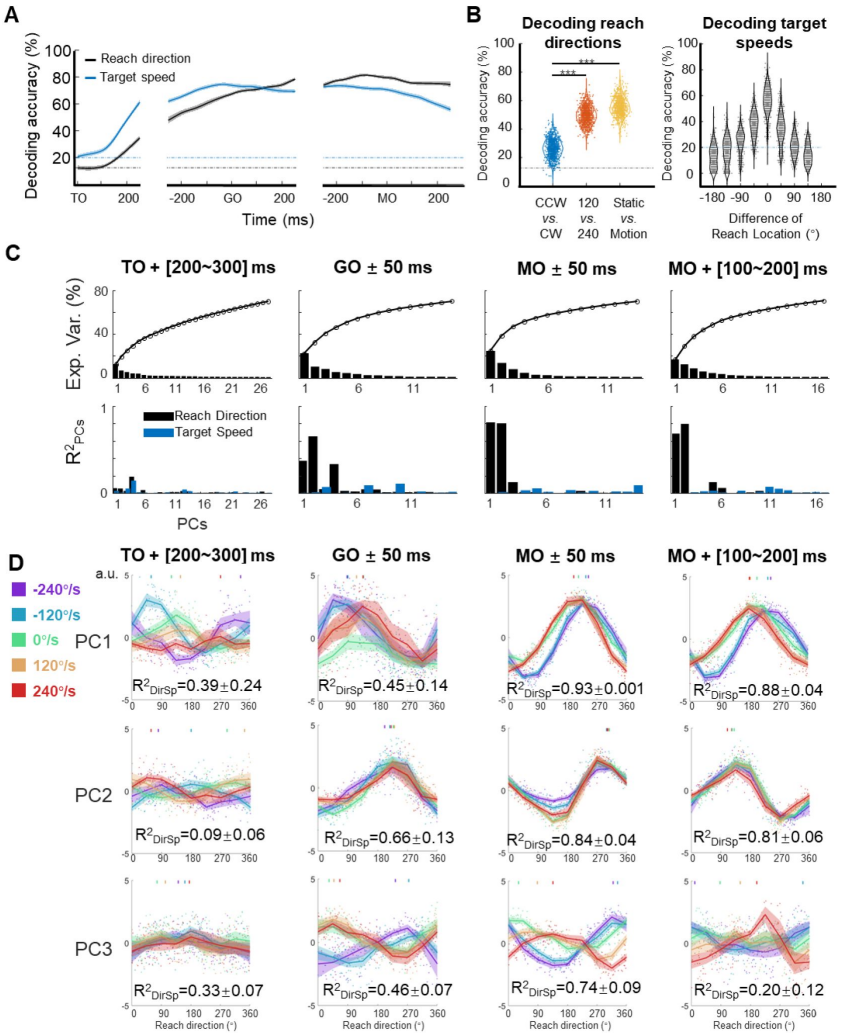

Figure 2.

Features of encoding pattern at population level

A The decoding accuracy (SVM with 10-fold cross-validation) of reach direction (black line) and target speed (blue line) by population activity (monkey C, n=95, 772 trials), is aligned to target on (TO), GO, and movement onset (MO). The dash-dotted lines are chance level of decoding reach direction (black, one in eight) and target speed (blue, one in five). The shaded area is the standard deviation of the decoding accuracy for 10 repetitions.

B The left panel shows the performance of reach-direction decoder (one in eight) transferred between different target-motion conditions. The SVM decoder was built on randomly selected 100 trials in training dataset and tested in another 100 trials from a dataset of different conditions (CCW *vs*. CW, 120 *vs*. 240, static *vs*. motion). The distributions of decoding accuracy were from 1000 repetitions and compared with one tailed t-test ($p<0.01$, with three stars). The right panel shows the performance of target-speed decoder (one in five) in different reach-direction conditions. In this case, reach direction is grouped by eight equal sectors (each 45°), and for each condition 60 trials were randomly selected for training and testing. The accuracy distribution was also obtained from 1000 repetitions.

C The principal components explained variance and representation. The first row shows the explained variance of each PC (cumulatively over 70%). The second row shows the PCs' fitting goodness (R^2_{PCs}) of reach direction and target speed in four epochs.

D The principal components represented target-speed modulated reach direction. Each row shows the directional tuning of one PC (the first three PCs in **C**) in four epochs. Each dot represents a trial, and tuning curves are averaged in eight reach directions, and PDs of PCs are short lines in the upside of subplot by a weighted sum of response. Legends are colored in five target-motion conditions. The goodness of fitting reach direction (R^2_{DirSp}) for the single-trial PCs under single target-motion conditions is shown by mean ± sd.

evident in the PC2-PC3 subspace (**Figure 3A** bottom and **Figure 3B** right). Note that here we performed an linear transformation on all resulting neural state points to make the ellipse of the static condition orthogonal to the z-axis for better visualization.

Next, we quantified the spatial features of these ellipses by calculating the tilting angles, which were between the normal vectors of the moving-target and static-target conditions. Strikingly, this tilting angle was linearly correlated with target speed (both TS_{mag} and TS_{dir}), and the relationship was robust in nine datasets from three monkeys (**Figure 3C** and Figure S9).

Given these results, we propose that this orbital neural geometry epitomizes the sensorimotor dynamics of M1 at the population level. The sensory input can regularly modulate neural states in an orthogonal dimension (PC3), without interfering with motor generation (in PC1 and PC2).

Population neural geometry relies on neuronal tuning

We then asked whether a group of single neurons with a certain type of mixed sensorimotor selectivity could exhibit the orbit neural geometry.

For this purpose, three neuronal models were constructed for the three typical modulations described above (PD shift, gain, and addition, see **Figure 1D** and Figure S2-S4). We ran a simulation with these representational neuronal models (**Figure 4A**). Here, each group consisted of 300 model neurons with their PDs uniformly distributed, and was solely modulated as PD-shift, gain, or addition (Methods). The resulting neural geometry of the three simulation groups showed distinct features (**Figure 4B**): The single-condition ellipses were inclined with target-motion-dependent angles in the PD-shift and gain groups, similar to the real neural data, but the ellipses in the addition group were layered in parallel. The reach-direction clusters in the first two PCs were conservative in the gain and addition group, but not in the PD-shift group. These results indicate that the neural states of the real data mainly exhibit the geometry feature of the gain modulation group. Nonetheless, we found that a population with a uniform mixture of all three modulations was able to simulate the neural geometry as well (**Figure 4C**).

Comparing with the static-target condition, we calculated relative rotation angle and tilting angle between ellipses along with the vertical shift of neural states, in order to quantify the simulated structure (**Figure 4D**). The results show that the real data yielded a smaller rotation angle than the PD-shift group, a smaller vertical shift than the additive group, but larger tilting angles than all models. The mixed group had the most similar tilting angle, though with moderate performance in rotation angle and state shift.

These simulations suggest that the existence of PD-shift and additive modulation would not disrupt the neural geometry that is primarily driven by gain modulation; rather it is possible that these three modulations support each other in a mixed population.

Recurrent neural network provides dynamic insights

To infer how such modulated subpopulations would interact with each other in a dynamical system, we trained 100 RNN models with random weight initialization (**Figure 5A**; see Methods). The inputs included motor intention, target location, and a Go signal. Motor intention was defined as an abstract motor command predicted to compensate for sensorimotor delays[28], and could be provided by the PPC[29,30], here simplified as the interception location. The network was to generate hand velocity after MO. For a fixed validation set of 500 trials, these trained network models performed well (mean square error of the reach endpoint and the target was 0.0046 ± 0.0027, a. u., mean ± sd., while the radius of target motion was 0.15).

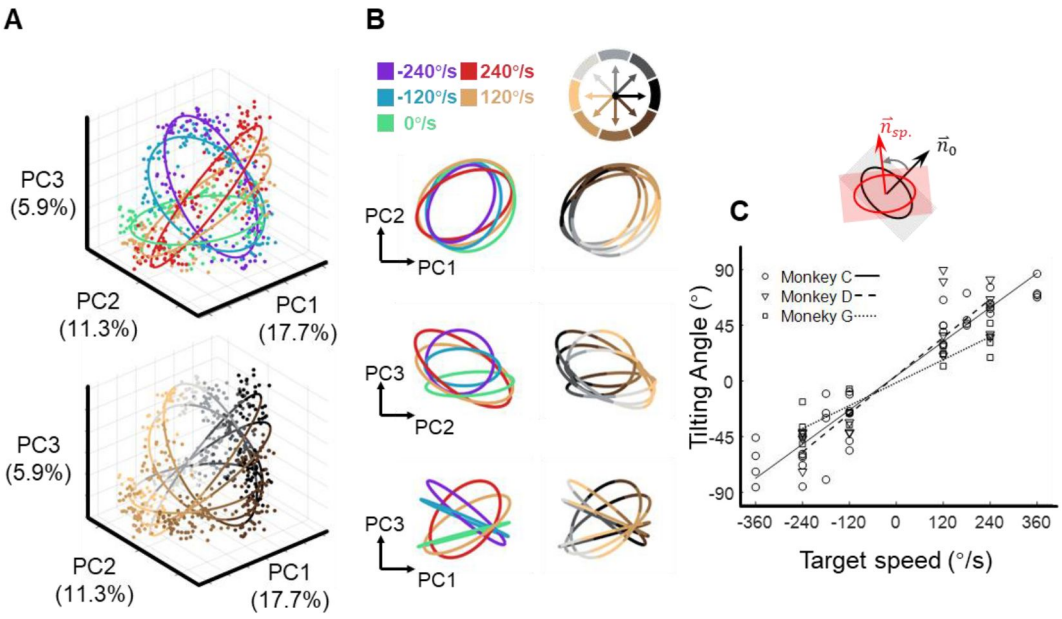

Figure 3.

The orbital neural geometry in latent dynamics

A Three-dimensional neural state of M1 activity obtained from PCA. As in **Figure 3c**, each point represents a single trial. The upper subplot is colored according to five target speeds, while the bottom is in colors corresponding to eight reach directions. The explained variances of the first three PCs were 17.7%, 11.3%, and 5.9%. Neural data were collected with target-speed modulated units (monkey C, N=480, merged six sessions) and random 15 trials in 40 conditions (K=600 trials).
B Fitted ellipses of neural states. The ellipses fitted in [A] are projected onto three two-dimensional spaces, colored in target speeds (left column) or reach directions (right column).
C The relative angle of ellipses. The angle is calculated between ellipses of the target-motion condition and static-target condition (0 °/s) in the range from -90° to 90°, CCW is positive. Circles, squares, and triangles correspond to monkeys C (7 sessions), G (4 sessions) and D (4 sessions), respectively. The lines represent the linear relationship of ellipses angle (θ) and target speed (sp.), with function solid line θ = 0.23*sp.+4.2, R_2=0.91 for monkey C; dashed line θ = 0.26*sp.+4.3, R_2=0.81 for monkey D; dotted line θ = 0.15*sp.-1.4, R_2=0.89 for monkey G.

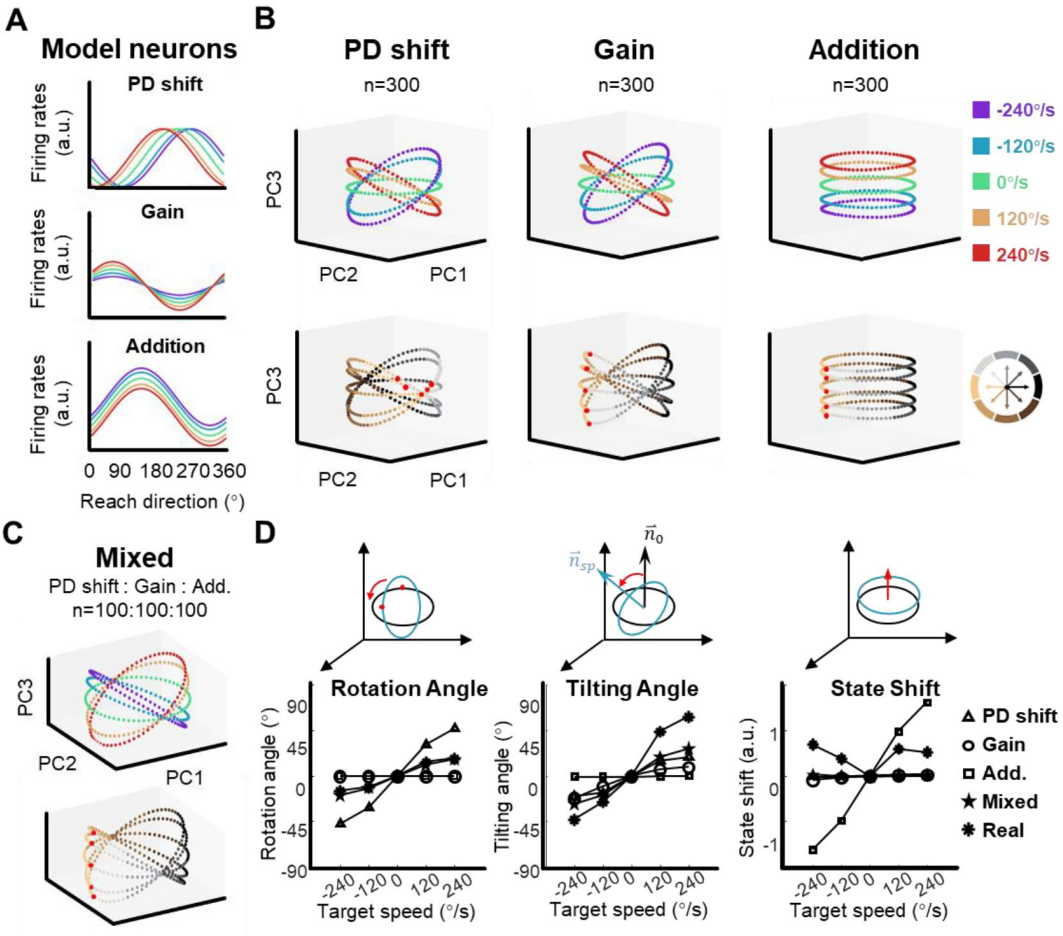

Figure 4.

The shape of neural dynamics relies on neuronal mixed selectivity

A The tuning curves of three ideal neurons in five target-motion conditions. From up to down, they are PD shift, gain modulation, and (offset) addition. The activity of these ideal neurons is simulated by the multiplication of temporal Gaussian function (bin=50 ms) and the reach-direction cosine function, also scaled by a sigmoid function involving target speed in three different ways.

B The simulated neural states from three groups, colored by target-motion conditions (first row) and reach directions (second row). For each simulation, the neural states were obtained from 300 model neurons by PCA. The neural state in 180° reach direction is highlighted with a red marker. The first two principal components can explain more than 95% of the variance in the data (the explained variance of the first three PCs, Gain: 49.5%, 46.6%, and 2.0%; PD shift: 50.1%, 47.1%, and 1.6%; Addition:50.8%, 47.9%, and 1.4%)

C The neural states of a mixed group of 100*3 model neurons, as in **B**. The explained variance of the first three principal components were 48.4%, 44.2%, and 3.1%.

D Quantification of the difference between neural-state ellipses in four simulated groups and a real dataset (monkey C, n=95). Rotation angle is the relative rotation angle differences in the first two neural state. Tilting angle is the relative angle of the normal vector of ellipses. State shift is the root mean square of the distance between two ellipses.

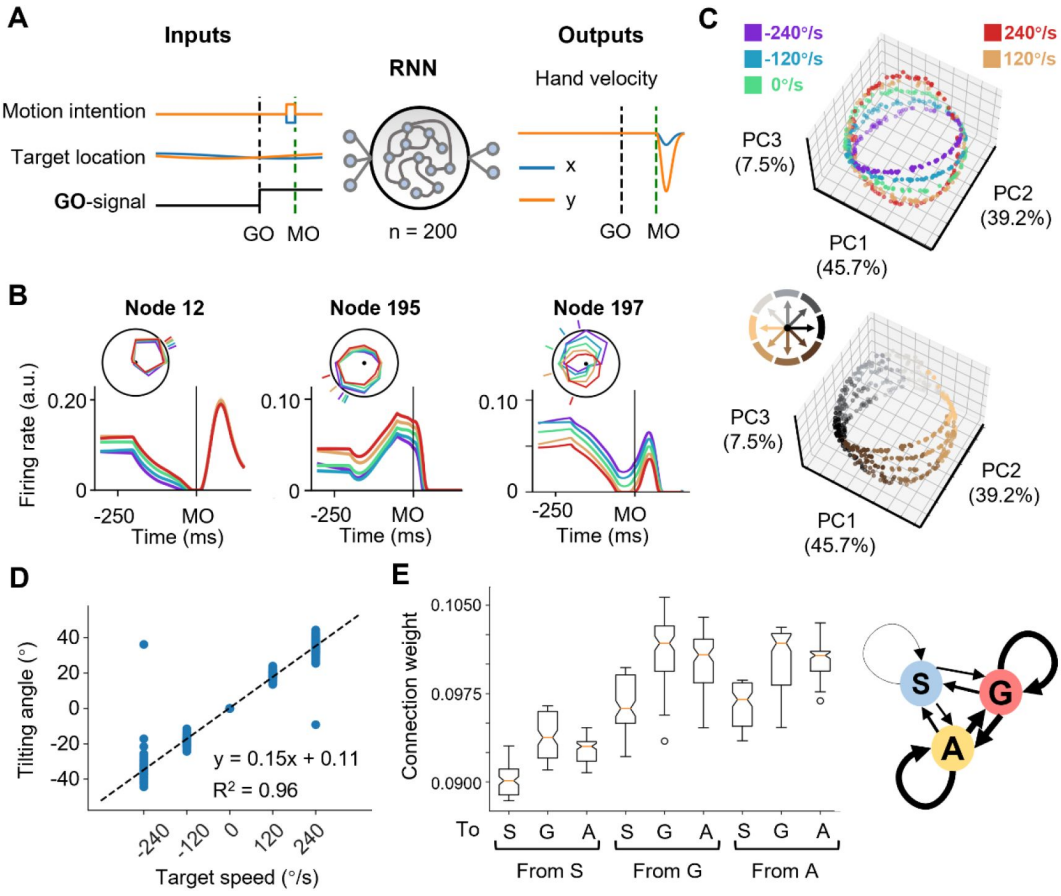

Figure 5.

The neural geometry in RNNs

A Network architecture. The network input consists of motor intention, target location, and GO signal. The motor intention is the two-dimensional Cartesian coordinates of the interception location, and exists fixed during MO-50ms to MO; the target location is the two-dimensional Cartesian coordinates of the moving target, and appears time-varying during the whole trial; the GO-signal is a step function from 0 to 1 after GO. The RNN with 200 hidden units is expected to output hand velocity as two-dimensional Cartesian coordinates for accurate interception.
B Three example nodes with PD-shift modulation, gain modulation, and addition modulation. Similar to **Figure 1D**.
C Three-dimensional neural state of node activity obtained from PCA, colored in target-motion conditions (top) and in reach-direction conditions (Bottom). Similar to **Figure 3A**.
D The relative angle of ellipses. Similar to **Figure 3D**. The fitted line is $\theta = 0.15*sp. +0.11$, $R^2 = 0.96$ for five target speeds.
E The connectivity between different types of modulations. On the left is a boxplot representing the averaged absolute connection weight, across 100 models. S for PD-shift nodes, G for gain nodes, and A for addition nodes. On the right is a diagram of the connectivity, with linewidth representing the connection strength.

In these network models, we found comparable features of nodes. First, most activated nodes (for example, **Figure 5B**) could be classified into the above-mentioned three modulations (**Table 1**) by the same statistical standard as for the real neural data. Second, the states reduced from node population activity were arranged in a way resembling the actual neural geometry at MO (the fitting goodness of ellipses, R_2 = 0.98 ± 0.05, mean ± sd.; **Figure 5C**). The tilting angles followed the same pattern as suggested by the actual results (**Figure 5D**).

With these RNN models, we perturbed the connection between different modulation groups. The connections within and between gain modulation and additive modulation were stronger than the others (**Figure 5E**), however, further strengthening the connection from gain to additive nodes or within additive nodes would disorder the orbital structure more significantly (Figure S10A and Table S2). We speculate that the influence, and perhaps the formation, of modulations both relate to the robust input and output weight pattern across models (Figure S10B, C). These results support strong and similar roles of gain and additive nodes, but what is even more important is that the three modulations interact each other, so the PD-shift nodes should not be neglected.

Discussion

To reveal how sensory context influence neural dynamics during movement, we recorded M1 population activity from monkeys performing a flexible manual interception that is highly dependent on predictive sensorimotor transformations. Single-neuron activity showed that the movement tuning of M1 neurons varied with target-motion conditions in complicated ways, including PD shift, gain modulation, addition, or their mixtures. Unsupervised dimensionality reduction (PCA) on population activity revealed an orbital neural geometry, where neural states of single trials spontaneously formed ellipses and were tilted according to target-motion conditions. Such a geometry, which could be simulated with a group of representational neurons for gain modulation alone, also emerged in the RNN with appropriate input-output mappings. As suggested by a dynamic and connected population as the RNN, the interactions between modulations were sophisticated in preserving the encoding of motor output. These results reveal sensory modulation of pre-movement neural dynamics at the single-neuron and population levels, and bridge the neuronal mixed sensorimotor selectivity and a low-dimensional neural geometry, compactly representing the sensorimotor co-function.

Previous studies have showed that M1 activity is seldom evoked by purely visual stimuli, with only weak tuning[8,31,32], and has transient responses to behaviorally relevant visual cues[7,10,33–35]. In this study, the modulated neural dynamics, though distinguished according to target-motion conditions, is ultimately shaped for motor generation rather than sensory representation. It is a pity that we did not record sufficient muscle data during interception to rule out the representation of the motor cortex for kinetic variables such as force[1,27,36], but we believe that this would not invalidate our main conclusions.

Previous studies have revealed interactions between motor kinematic variables such as reach direction and hand velocity[15,37,38]. Although the effect of arm-dependent speed (hand velocity) on reach-direction tuning may exist, it cannot fully explain neural activity during interception. First, we found hand velocity to vary with TS_{mag}, but the largest gap in neuronal activity was related to TS_{dir}. Second, for a new dataset with trials resampled to ensure similar distributions of hand velocities in five target-motion conditions, the orbital neural geometry remained similar and the target-motion gain model provided a better explanation compared to the hand-velocity gain model (Figure S11).

In the present study, we focused on the orbital neural geometry by taking ‘snapshots’ of neural activities with PCA. In addition to unsupervised PCA, we tried supervised dimensionality reduction methods like dPCA[24]. However, the dPCA results (Figure S7) showed that the condition-

independent temporal component explained the largest variance, followed by the component of reach direction, whereas the interactive and target-speed components only covered very small proportions. The dPCA did not distinguish a target-speed dimension, probably because reach directions were continually distributed around a circle and target speed was primarily mixed with reach directionality.

Our simulations with neuronal models and RNN demonstrate that differences in modulations and the interaction between them can be essential. In fact, modulations in the form of PD shift and gain have been widely found in the motor cortex and PPC regions contributing to sensorimotor transformation. For example, motor cortex neurons experience gain and PD shift modulation by arm posture[36,39,40]. Neurons in PPC have eye and hand gain fields for a visually-guided reach plan[41–43], integrating target position related to gaze and hand position to form motor intention[29,44,45]. Therefore, we conclude that three types of modulations should all be involved in sensorimotor computation in predictive motor control. In addition, recent studies show that interactions of PPC-motor cortex circuity are involved in motor planning, spatial transformation and motor selection[46–48]. The PPC-M1 circuit, as a key part of cortico-subcortical networks for the predictive sensorimotor control[49], is a topic for future studies.

STAR Methods

Key resources table

REAGENT or RESOURCE	SOURCE	IDENTIFIER
Experimental models: Organisms/strains		
Rhesus macaques (Macaca mulatta)	Beijing Institute of Xieerxin Biology Resource, China	N/A
Software and algorithms		
Matlab	MathWorks	http://mathworks.com/
Python		
Other		
Cerebus System	Blackrock Microsystems	https://blackrockneurotech.com/products/cerebus/
Utah Microelectrode Arrays	Blackrock Microsystems	https://blackrockneurotech.com/products/utah-array/

Resource availability Lead contact

Further information and requests for resources and reagents should be directed to and will be fulfilled by the Lead Contact, Dr. He Cui (**hecui@cibr.ac.cn**).

Materials availability

This study did not generate new unique reagents

Data and code availability

The example datasets and code have been deposited in Mendeley Preview, and will be made public as soon as the article is officially published.

Experimental model and study participant details

Monkey

Three adult male rhesus macaques (monkey C, D, and G, *Macaca mulatta*, 7-10 kg) were used in this study. The monkeys sat in a primate chair to perform the task. The stimuli were back projected onto a vertical touch screen (Elo Touch system; sampling at 100 Hz, spatial resolution <0.1 mm) about 30 cm in front of the monkeys. Hand trajectory was tracked by an optical camera (VICON Inc.) with an infrared marker on the fingertip. All animal maintenance and procedures were in accordance with NIH guidelines and approved by the Institutional Animal Care and Use Committee (IACUC) of Institute of Neuroscience, CAS.

Method details

Task and behavior

The monkeys were trained to perform a flexible manual interception task in a dark room. The task paradigm was modified based on the visually-guided reaching interception task in a previous study [22]. At the beginning, the monkey held the green center dot of a touch screen for 600 ms to initiate a trial (**Figure 1A**). Then, a green target dot appeared at a random location, moving in a circular path centered on the center dot. The center dot turned dark as a GO cue after a random delay (400-800 ms); then the monkey could intercept the target at any moment within 150-800 ms after the GO cue. Once any peripheral location was touched, the target stopped. The tolerance range of the touch endpoint for correct trials was within 3 cm of the target. The monkey would be rewarded with juice after each correct trial. Targets moving clockwise (CW; -240 °/s, -120 °/s) and counterclockwise (CCW; 120 °/s, 240 °/s), as well as a stationary target (0°/s), were pseudo-randomly interleaved trial by trial. Additional target speeds (-360 °/s, -180 °/s, 180 °/s, 360 °/s added) were introduced in subsequent sessions (Table S1).

Data collection

After the monkeys were adequately trained for the task (successful rate > 90%), head-posts were implanted stereotaxically under anesthesia (induced by 10 mg/kg ketamine, then sustained by 2% Isoflurane). After few weeks of recovery and adaptation, the monkeys were implanted with Utah microelectrode arrays (Blackrock Microsystems, Salt Lake City, UT) in the motor cortex of the hemisphere contralateral to the handedness (**Figure 1C**, 128-channel array for monkey C, 96-channel array for monkey G and D). The location of recording areas were identified by Magnetic Resonance Imaging (MRI) and cortical sulcus features. Neuronal activity was recorded via a Blackrock Microsystem 256-channel recording system, sampled at 30 kHz. We collected 85 ± 16, 45 ± 8, 98 ± 18 well-isolated units from monkey C, G, and D across sessions (mean ± sd. more details in Table S1), respectively.

Peri-stimulus time histograms (PSTHs)

The PSTHs and spike rasters of single neurons are shown in **Figure 1D** and Figure S2-S4. All trials were classified into forty conditions, eight reach-endpoint sectors by five target-motion conditions. Condition-averaged firing rates were calculated with 50-ms bins and smoothed with a Gaussian kernel (standard deviation = 20 ms). The standard error of firing rates was estimated from the 10 bootstrap samples in the trials of corresponding condition.

Quantification and statistical analysis

Classification of neuronal tuning properties

To classify target-motion modulation for single neuron reach-direction tuning, we used the direction-averaged firing rate around movement onset (MO ± 100ms) to calculate three indexes for each target-motion conditions: the preferred direction (PD), the tuning depth, and the offset activity, and classified PD shift, gain, and addition groups in **Table 1**. The PD of each neuron for different target-motion conditions was calculated by the weighted sum of averaged neuronal firing rates in eight reach-direction sectors. The tuning depth of each neuron was determined by the range (max - min) of firing rates in corresponding target-motion conditions. The offset activity of each neuron was calculated by the mean firing rate (MO ± 100 ms) of all target-motion conditions.

Based on the PD, tuning depth and offset activity of single neurons, a neuron was classified as 'PD shift', if its PDs were significantly different between interception and static-target condition (Watson-Williams test in circular data, CircStat by[50]); a neuron was classified as 'gain' if its tuning depths were significantly different between interception and static-target condition (two-tailed Wilcoxon signed-rank test, $p<0.05$); a neuron was classified as 'offset' if its offset activities were significantly different between interception and static-target condition (two-tailed Wilcoxon signed-rank test, $p<0.05$).

Population decoding

The population activity of the motor cortex was used to decode target motion and reach direction by support vector machine (SVM). Neuronal firing rate was soft-normalized as

$$FR_{norm.} = \frac{FR_{raw}}{FR_{max} - FR_{min} + 5}$$

where raw firing rates was divided by the range of firing rates plus five [18]. We trained two SVM classifiers (MATLAB function 'fitcecoc', 10-fold cross-validation) to decode reach direction (one in eight) and target motion (one in five) of single trials in 100-ms window sliding with 50-ms step (**Figure 2A**). The temporal decoding was repeated ten times to obtain the mean and standard deviation of decoding accuracy.

We tested the generalization of reach-direction and target-motion decoders (SVM, MATLAB function 'fitcecoc') in different conditions during execution period (MO ± 100 ms, **Figure 2B**). The decoder predicted single-trial reach direction (45°, 1/8 chance level) or target motion (1/5 chance level) across conditions based on normalized population activity. The reach-direction decoder (**Figure 2B** left), which was trained by trials in a set of target-motion conditions, was tested with trials from other target-motion conditions (CCW vs. CW, or 120 vs. 240, or static vs. motion, randomly selected without replacement 100 trials from corresponding training-test datasets), and the training-test decoding was repeated 1000 times to compare the distribution of accuracy with paired t-test. The target-speed decoder (**Figure 2B** right), which was trained by trials in a given reach-direction condition within 45°, was tested with trials from other reach-direction conditions.

Neural state

The population activity was stored in NKT datasets, where N, K, and T denote the number of neurons, trials, and time bins, respectively. We averaged T dimension of neural activity in a 100-ms bin (e.g., the two 50-ms bins around MO), and normalized neuronal dimension by Z-score (MATLAB function 'zscore') to get a K*N dataset. After preprocessing, we used PCA to reduce the

dimension from K*N to K*C (C is the number of principal components, first two and first three PCs), and fitted the PCs with reach direction ($PC = a_1{*}cos(\theta){+}a_2{*}sin(\theta){+}c$) and target speed ($PC = \frac{a_1}{1+e^{-a_2(sp.)}} + c$) in **Figure 2**. Neural states of single trials were colored for target speed or reach direction and fitting ellipses with first two PCs (**Figure 2D**) and first three PCs (**Figure 3**) by MATLAB package 'MatGeom'[51]. To show the relative position of ellipses in the best viewing angle, we used an isometric affine transformation to globally map all datapoints on new axes while preserving the proportional relation of distances between points. After this linear transformation, the azimuth and elevation of ellipses changed slightly, but the tilting angle between ellipses remained constant (**Figure 3**). The tilting angles, rotation angles, and state shift were calculated between ellipses of target-motion conditions and static-target condition in each session, defining CW as negative angles and CCW as positive angles. A set of tilting angles were obtained from corresponding conditions in one dataset, and the linear regression model was used to fit all ellipses angles (θ) and target speeds (sp.) in nine sessions.

Fitting and simulating single-neuron activity

We used PD shift, gain, offset, and full models to fit neuronal activity, basing on a cosine tuning model[3]. Neurons are fitted by single-trial data. We introduced a special sigmoid function to fit the nonlinear target-speed effects because target-speed direction (CCW vs. CW) has a stronger effect than target-speed magnitude (120 vs. 240)[52,53]. The gain and additive models refer to hand-velocity gain studies[37,38,54].

In the gain model, the target-speed effects on the amplitude of cosine tuning are denoted as:

$$FR = \left(\frac{a_1}{1+e^{-a_2(sp.)}} + c_2\right) * cos(\theta - \theta_{pd}) + c_1$$

where FR is the firing rate at movement onset (MO ± 100 ms). θ and $sp.$ are the reach direction and target speeds, respectively; θ_{pd} is the fitted preferred direction of the neuron; a_1, a_2, c_1 are constants to be fitted.

In the additive model, the target speed adjusts the offset activity, as:

$$FR = a_1 * cos(\theta - \theta_{pd}) + \frac{a_3}{1+e^{-a_2(sp.)}} + c_1$$

with similar symbols to the gain models, plus the new constant a_3.

In the PD shift model, the target-speed effects on PDs are represented as:

$$FR = a_1 * cos\left(\theta - \theta_{pd} + \frac{a_3}{1+e^{-a_2(sp.)}}\right) + c_1$$

with the similar symbols to the above model.

The full model integrates all the three of the above effects:

$$FR = a_1 * cos(\theta - pd_{sp}) + \frac{a_2}{1+e^{-a_2(sp.)}} + \frac{a_3}{1+e^{-a_2(sp.)}} * cos(\theta - pd_{sp}) + a_4 * cos\left(\theta - pd_{sp} - \frac{a_5}{1+e^{-a_2(sp.)}}\right) + c_1$$

with constants a_1, a_2, a_3, a_4, a_5.

We fitted neuronal activity with these four models (MATLAB 'fit' function), and compared the fitting goodness with adjusted R-squares $R^2_{adj.} = \frac{(1-r^2)(n-1)}{n-p-1}$, where n is the trial number, and p is the degree of the polynomial).

Simulations with model neurons were based on three models to investigate the relationship between neuronal tuning (**Figure 4A**) and population neural geometry (**Figure 4B**). We first built three model neuron groups (each n=300) and performed PCA to get the neural state. Then, we repeated this in a mixed group, with 100 each of PD shift, gain and additive model neurons (**Figure 4C**). Model neurons had three components: cosine-tuning for reach direction ($\theta_{pd,n}$, PD uniform distribution around circle for each neuron n), Gaussian temporal profiles (t=1:200, σ=30, peak time $t_{\mu,n} \in N(100, 10)$, the 100-th bin is MO, random distribution for $t_{\mu,n}$ of neurons), and distinct target-motion modulation for each group. We designed five target speed values ($sp.$ = [1,2,3,4,5]) and 64 reach directions $(\theta = 360 * \frac{[1:64]}{64})$, for 320 trials in total[55].

The gain-model neuron has a nonlinear function with target-speed effects on the amplitude:

$$FR_{t,n,sp.,\theta} = e^{\frac{-(t-t_{\mu,n})^2}{2*30^2}} * \left(\frac{1}{1+e^{-g_n(sp.-3)}} * cos(\theta - \theta_{pd,n}) + 1\right)$$

where g_n is a random target-motion gain within [0:1] for different neurons, and modulates targetmotion gain in a sigmoidal function.

The PD-shift model neuron has target-speed change in PD:

$$FR_{t,n,sp.,\theta} = e^{\frac{-(t-t_{\mu,n})^2}{2*30^2}} * \left(cos\left(\theta - \theta_{pd,n} - \frac{90}{1+e^{-s_n(sp.-3)}}\right) + 1\right)$$

where s_n is a random value within [0:1.5] for different neurons, and contributes to a sigmoidal function with target-motion shift on neuronal PD ($\theta_{pd,n}$).

The additive model neuron has target-speed effects in offset:

$$FR_{t,n,sp.,\theta} = e^{\frac{-(t-t_{\mu,n})^2}{2*30^2}} * \left(cos(\theta - \theta_{pd,n}) + \frac{1}{1+e^{-g_n(sp.-3)}} + 1\right)$$

where g_n is also a random value within [0:1] for different neurons, and adjusts the offset activity in a sigmoidal function with target-motion.

The firing rates of three groups model neuron (K*N*T, 320*300*200) were averaged at MO (mean T = [50:150]) to get the K*N (320*200) dataset for PCA. As with the real neural data, we selected the first three PCs (K*C, 320*3) to derive the simulated neural state shown in **Figure 4**.

RNN training

For the inputs of RNN, motor intention appeared from MO-50 ms to MO, and was represented as constant variables in the form of two-dimensional Cartesian coordinates; target location was designed as time varying two-dimensional Cartesian coordinates of the target throughout the entire trial; the Go-signal was a step function jumping from 0 to 1 at GO. The RNN consisted of 200 hidden units, and output hand velocity for accurate interception after MO.

The RNN nodes evolved according to a standard dynamic differential equation:

$$\tau\dot{x} = -x + Jr + Bu$$

where τ is a time constant (here 50 ms), x is the activity, r is the firing rates, and u means the combined inputs. The connection matrix J of hidden layer is initiated as random in a normal distribution (mean = 0, $\text{sigma} = g/\sqrt{N}$, g = 1.5, N = 200), and the matrix B denotes the connection between inputs and hidden units, initiated as zero matrix. The output z is obtained by

$$z = Wr$$

where W is the read-out weight, and is expected to reproduce the desired hand velocity generated by bell-shaped physical equation[56]. W was also initiated as zero matrix. During training, the loss function was:

$$E = e + \alpha r_1$$

where e is the mean squared error of z and training target. r_1 is regularity [57], denoting the magnitude of the nodes' activity and is calculated as activity squared summed across time. For constants, $\alpha = 1e-7$. The optimization was realized with optim.Adam() based on PyTorch, the learning rate was 0.001.

The classification of nodes' modulation type was finished with the same procedure for real data as above. When perturbating the connection between certain types of modulations, the selected connection was multiplied with 1.5. This perturbation was retained for the entire trial. The perturbed network was tested with the same test set of 500 trials as for the intact network.

Acknowledgements

We thank C. Li, J. Malpeli, C. Zheng, and R. Zheng for helpful comments and discussions; C. Guan for veterinary assistance; and P. Ding, L. Du, and Z. Xiao for administrative support. This work was supported by the National Key R&D Program (Grants 2020YFB1313400 and 2017YFA0701102), National Science Foundation of China (Grants 31871047 and 31671075), and CAS Strategic Priority Research Program (Grant XDB32040103).

Author contributions

Y. Zhang and H. Cui designed the experiment, Y. Zhang and T. Wang collected the data, Y. Zhang and Y. Chen analyzed the data, Y. Chen built RNNs, Y. Zhang performed the simulation, Y. Zhang, Y. Chen, T Wang, and H. Cui prepared the manuscript.

Declaration of interests

The authors declare no conflict of interests.

References

1. Evarts E. V (1968) **Relation of pyramidal tract activity to force exerted during voluntary movement** *J. Neurophysiol* **31**:14–27 https://doi.org/10.1152/jn.1968.31.1.14

2. Tanaka H. (2016) **Modeling the motor cortex: Optimality, recurrent neural networks, and spatial dynamics** *Neurosci. Res* **104**:64–71 https://doi.org/10.1016/j.neures.2015.10.012

3. Georgopoulos A., Kalaska J., Caminiti R., Massey J. (1982) **On the relations between the direction of two-dimensional arm movements and cell discharge in primate motor cortex** *J. Neurosci* **2**:1527–1537 https://doi.org/10.1523/JNEUROSCI.02-11-01527.1982

4. Omrani M., Kaufman M.T., Hatsopoulos N.G., Cheney P.D. (2017) **Perspectives on classical controversies about the motor cortex** *J. Neurophysiol* **118**:1828–1848 https://doi.org/10.1152/jn.00795.2016

5. Wang T., Chen Y., Cui H. (2022) **From Parametric Representation to Dynamical System: Shifting Views of the Motor Cortex in Motor Control** *Neurosci. Bull* https://doi.org/10.1007/s12264-022-00832-x

6. Rizzolatti G., Scandolara C., Matelli M., Gentilucci M. (1981) **Afferent properties of periarcuate neurons in macaque monkeys** *II. Visual responses. Behav. Brain Res* **2**:147–163 https://doi.org/10.1016/0166-4328(81)90053-X

7. Lamarre Y., Busby L., Spidalieri G. (1983) **Fast ballistic arm movements triggered by visual, auditory, and somesthetic stimuli in the monkey. I. Activity of precentral cortical neurons** *J. Neurophysiol* **50**:1343–1358 https://doi.org/10.1152/jn.1983.50.6.1343

8. Merchant H., Battaglia-Mayer A., Georgopoulos A.P. (2001) **Effects of Optic Flow in Motor Cortex and Area 7a** *J. Neurophysiol* **86**:1937–1954 https://doi.org/10.1152/jn.2001.86.4.1937

9. Merchant H., Battaglia-Mayer A., Georgopoulos A.P. (2004) **Neural responses in motor cortex and area 7a to real and apparent motion** *Exp. Brain Res* **154**:291–307 https://doi.org/10.1007/s00221-003-1664-5

10. Rao N.G., Donoghue J.P. (2014) **Cue to action processing in motor cortex populations** *J. Neurophysiol* **111**:441–453 https://doi.org/10.1152/jn.00274.2013

11. Hatsopoulos N.G., Suminski A.J. (2011) **Sensing with the Motor Cortex** *Neuron* **72**:477–487 https://doi.org/10.1016/j.neuron.2011.10.020

12. Sobinov A.R., Bensmaia S.J. (2021) **The neural mechanisms of manual dexterity** *Nat. Rev. Neurosci* **22**:741–757 https://doi.org/10.1038/s41583-021-00528-7

13. Suway S.B., Schwartz A.B. (2019) **Activity in Primary Motor Cortex Related to Visual Feedback** *Cell Rep* **29**:3872–3884 https://doi.org/10.1016/j.celrep.2019.11.069

14. Pesaran B., Nelson M.J., Andersen R.A. (2006) **Dorsal Premotor Neurons Encode the Relative Position of the Hand, Eye, and Goal during Reach Planning** *Neuron* **51**:125–134 https://doi.org/10.1016/j.neuron.2006.05.025

15. Paninski L., Fellows M.R., Hatsopoulos N.G., Donoghue J.P. (2004) **Spatiotemporal Tuning of Motor Cortical Neurons for Hand Position and Velocity** *J. Neurophysiol* **91**:515–532 https://doi.org/10.1152/jn.00587.2002

16. Cisek P., Kalaska J.F. (2005) **Neural Correlates of Reaching Decisions in Dorsal Premotor Cortex: Specification of Multiple Direction Choices and Final Selection of Action** *Neuron* **45**:801–814 https://doi.org/10.1016/j.neuron.2005.01.027

17. Tkach D., Reimer J., Hatsopoulos N.G. (2007) **Congruent Activity during Action and Action Observation in Motor Cortex** *J. Neurosci* **27**:13241–13250 https://doi.org/10.1523/JNEUROSCI.2895-07.2007

18. Churchland M.M., Cunningham J.P., Kaufman M.T., Foster J.D., Nuyujukian P., Ryu S.I., Shenoy K. V (2012) **Neural population dynamics during reaching** *Nature* **487**:51–56 https://doi.org/10.1038/nature11129

19. Shenoy K. V, Sahani M., Churchland M.M. (2013) **Cortical Control of Arm Movements: A Dynamical Systems Perspective** *Annu. Rev. Neurosci* **36**:337–359 https://doi.org/10.1146/annurev-neuro-062111-150509

20. Vyas S., Golub M.D., Sussillo D., Shenoy K. V. (2020) **Computation Through Neural Population Dynamics** *Annu. Rev. Neurosci* **43**:249–275 https://doi.org/10.1146/annurev-neuro-092619-094115

21. Merchant H., Battaglia-Mayer A., Georgopoulos A.P. (2004) **Neural Responses during Interception of Real and Apparent Circularly Moving Stimuli in Motor Cortex and Area 7a** *Cereb. Cortex* **14**:314–331 https://doi.org/10.1093/cercor/bhg130

22. Li Y., Wang Y., Cui H. (2018) **Eye-hand coordination during flexible manual interception of an abruptly appearing, moving target** *J. Neurophysiol* **119**:221–234 https://doi.org/10.1152/jn.00476.2017

23. Li Y., Wang Y., Cui H. (2022) **Posterior parietal cortex predicts upcoming movement in dynamic sensorimotor control** *Proc. Natl. Acad. Sci* **119** https://doi.org/10.1073/pnas.2118903119

24. Kobak D., Brendel W., Constantinidis C., Feierstein C.E., Kepecs A., Mainen Z.F., Qi X.-L., Romo R., Uchida N., Machens C.K. (2016) **Demixed principal component analysis of neural population data** *Elife* **5**:1–36 https://doi.org/10.7554/eLife.10989

25. Mante V., Sussillo D., Shenoy K. V., Newsome W.T. (2013) **Context-dependent computation by recurrent dynamics in prefrontal cortex** *Nature* **503**:78–84 https://doi.org/10.1038/nature12742

26. Parthasarathy A., Herikstad R., Bong J.H., Medina F.S., Libedinsky C., Yen S.C. (2017) **Mixed selectivity morphs population codes in prefrontal cortex** *Nat. Neurosci* **20**:1770–1779 https://doi.org/10.1038/s41593-017-0003-2

27. Sun X., O'Shea D.J., Golub M.D., Trautmann E.M., Vyas S., Ryu S.I., Shenoy K. V. (2022) **Cortical preparatory activity indexes learned motor memories** *Nature* **602**:274–279 https://doi.org/10.1038/s41586-021-04329-x

28. Cui H. (2016) **Forward Prediction in the Posterior Parietal Cortex and Dynamic Brain-Machine Interface** *Front. Integr. Neurosci* **10**:1–6 https://doi.org/10.3389/fnint.2016.00035

29. Andersen R.A., Buneo C.A. (2002) **Intentional maps in posterior parietal cortex** *Annu Rev Neurosci* **25**:189–220 https://doi.org/10.1146/annurev.neuro.25.112701.142922

30. Andersen R.A., Cui H. (2009) **Intention, Action Planning, and Decision Making in Parietal-Frontal Circuits** *Neuron* **63**:568–583 https://doi.org/10.1016/j.neuron.2009.08.028

31. Kwan H.C., Mackay W.A., Murphy J.T., Wong Y.C. (1985) **Properties of visual cue responses in primate precentral cortex** *Brain Res* **343**:24–35 https://doi.org/10.1016/0006-8993(85)91154-0

32. Kruse W. (2002) **Temporal Relation of Population Activity in Visual Areas MT/MST and in Primary Motor Cortex during Visually Guided Tracking Movements** *Cereb. Cortex* **12**:466–476 https://doi.org/10.1093/cercor/12.5.466

33. Alexander G.E., Crutcher M.D. (1990) **Neural representations of the target (goal) of visually guided arm movements in three motor areas of the monkey** *J. Neurophysiol* **64**:164–178 https://doi.org/10.1152/jn.1990.64.1.164

34. Lurito J.T., Georgakopoulos T., Georgopoulos A.P. (1991) **Cognitive spatial-motor processes** *7. The making of movements at an angle from a stimulus direction: studies of motor cortical activity at the single cell and population levels. Exp. Brain Res* **87**:562–580 https://doi.org/10.1007/BF00227082

35. Port N.L., Kruse W., Lee D., Georgopoulos A.P. (2001) **Motor Cortical Activity during Interception of Moving Targets** *J. Cogn. Neurosci* **13**:306–318 https://doi.org/10.1162/08989290151137368

36. Scott S.H., Kalaska J.F. (1997) **Reaching Movements With Similar Hand Paths But Different Arm Orientations. I. Activity of Individual Cells in Motor Cortex** *J. Neurophysiol* **77**:826–852 https://doi.org/10.1152/jn.1997.77.2.826

37. Moran D.W., Schwartz A.B. (1999) **Motor Cortical Representation of Speed and Direction During Reaching** *J. Neurophysiol* **82**:2676–2692 https://doi.org/10.1152/jn.1999.82.5.2676

38. Inoue Y., Mao H., Suway S.B., Orellana J., Schwartz A.B. (2018) **Decoding arm speed during reaching** *Nat. Commun* **9**:1–14 https://doi.org/10.1038/s41467-018-07647-3

39. Kakei S., Hoffman D.S., Strick P.L. (1999) **Muscle and Movement Representations in the Primary Motor Cortex** *Science (80-* **285**:2136–2139 https://doi.org/10.1126/science.285.5436.2136

40. Kakei S., Hoffman D.S., Strick P.L. (2001) **Direction of action is represented in the ventral premotor cortex** *Nat. Neurosci* **4**:1020–1025 https://doi.org/10.1038/nn726

41. Batista A.P., Buneo C. a, Snyder L.H., Andersen R. a (1999) **Reach Plans in Eye-Centered Coordinates** *Science (80-* **285**:257–260 https://doi.org/10.1126/science.285.5425.257

42. Buneo C. a, Jarvis M.R., Batista A.P., Andersen R. a (2002) **Direct visuomotor transformations for reaching** *Nature* **416**:632–636 https://doi.org/10.1038/416632a

43. Chang S.W.C., Papadimitriou C., Snyder L.H. (2009) **Using a Compound Gain Field to Compute a Reach Plan** *Neuron* **64**:744–755 https://doi.org/10.1016/j.neuron.2009.11.005

44. Andersen R.A., Snyder L., Bradley D., Xing J. (1997) **Multimodal Representation of Space in the Posterior Parietal Cortex and Its Use in Planning Movements** *Annu. Rev. Neurosci* **20**:303–330 https://doi.org/10.1146/annurev.neuro.20.1.303

45. Cohen Y.E., Andersen R.A. (2002) **A common reference frame for movement plans in the posterior parietal cortex** *Nat. Rev. Neurosci* **3**:553–562 https://doi.org/10.1038/nrn873

46. Schaffelhofer S., Scherberger H. (2016) **Object vision to hand action in macaque parietal, premotor, and motor cortices** *Elife* **5**:1–24 https://doi.org/10.7554/eLife.15278

47. Dann B., Michaels J.A., Schaffelhofer S., Scherberger H. (2016) **Uniting functional network topology and oscillations in the fronto-parietal single unit network of behaving primates** *Elife* **5**:1–27 https://doi.org/10.7554/eLife.15719

48. Martínez-Vázquez P., Gail A. (2018) **Directed interaction between monkey premotor and posterior parietal cortex during motor-goal retrieval from working memory** *Cereb. Cortex* **28**:1866–1881 https://doi.org/10.1093/cercor/bhy035

49. Brozovič M., Gail A., Andersen R.A. (2007) **Gain mechanisms for contextually guided visuomotor transformations** *J. Neurosci* **27**:10588–10596 https://doi.org/10.1523/JNEUROSCI.2685-07.2007

50. Berens P. (2009) **CircStat : A MATLAB Toolbox for Circular Statistics** *J. Stat. Softw* **31**:128–129 https://doi.org/10.18637/jss.v031.i10

51. Legland D. **Legland, D. MatGeom library for geometric computing with MATLAB.**

52. Pouget A., Sejnowski T.J. (1997) **Spatial transformations in the parietal cortex using basis functions** *J. Cogn. Neurosci* **9**:222–237 https://doi.org/10.1162/jocn.1997.9.2.222

53. Churchland M.M., Lisberger S.G. (2001) **Shifts in the population response in the middle temporal visual area parallel perceptual and motor illusions produced by apparent motion** *J. Neurosci* **21**:9387–9402 https://doi.org/10.1523/jneurosci.21-23-09387.2001

54. Amirikian B., Georgopulos A.P. (2000) **Directional tuning profiles of motor cortical cells** *Neurosci. Res* **36**:73–79 https://doi.org/10.1016/S0168-0102(99)00112-1

55. Michaels J.A., Dann B., Scherberger H. (2016) **Neural Population Dynamics during Reaching Are Better Explained by a Dynamical System than Representational Tuning** *PLoS Comput. Biol* **12**:1–22 https://doi.org/10.1371/journal.pcbi.1005175

56. Kao T.C., Sadabadi M.S., Hennequin G. (2021) **Optimal anticipatory control as a theory of motor preparation: A thalamo-cortical circuit model** *Neuron* **109**:1567–1581 https://doi.org/10.1016/j.neuron.2021.03.009

57. Sussillo D., Churchland M.M., Kaufman M.T., Shenoy K. V (2015) **A neural network that finds a naturalistic solution for the production of muscle activity** *Nat. Neurosci* **18**:1025–1033 https://doi.org/10.1038/nn.4042

Editors

Reviewing Editor
Juan Alvaro Gallego
Imperial College London, London, United Kingdom

Senior Editor
Tamar Makin
University of Cambridge, Cambridge, United Kingdom

Reviewer #1 (Public Review):

Summary:

This study addresses the question of how task-relevant sensory information affects activity in the motor cortex. The authors use various approaches to address this question, looking at single units and population activity. They find that there are three subtypes of modulation by sensory information at the single unit level. Population analyses reveal that sensory information affects the neural activity orthogonally to motor output. The authors then compare both single unit and population activity to computational models to investigate how encoding of sensory information at the single unit level is coordinated in a network. They find that an RNN that displays similar orbital dynamics and sensory modulation to the motor cortex also contains nodes that are modulated similarly to the three subtypes identified by the single unit analysis.

Strengths:

The strengths of this study lie in the population analyses and the approach of comparing single-unit encoding to population dynamics. In particular, the analysis in Figure 3 is very elegant and informative about the effect of sensory information on motor cortical activity. The task is also well designed to suit the questions being asked and well controlled.

It is commendable that the authors compare single units to population modulation. The addition of the RNN model and perturbations strengthen the conclusion that the subtypes of individual units all contribute to the population dynamics. However, the subtypes (PD shift, gain, and addition) are not sufficiently justified. The authors also do not address that single units exhibit mixed modulation, but RNN units are not treated as such.

Weaknesses:

The main weaknesses of the study lie in the categorization of the single units into PD shift, gain, and addition types. The single units exhibit clear mixed selectivity, as the authors highlight. Therefore, the subsequent analyses looking only at the individual classes in the RNN are a little limited. Another weakness of the paper is that the choice of windows for analyses is not properly justified and the dependence of the results on the time windows chosen for single-unit analyses is not assessed. This is particularly pertinent because tuning curves are known to rotate during movements (Sergio et al. 2005 Journal of Neurophysiology).

This paper shows sensory information can affect motor cortical activity whilst not affecting motor output. However, it is not the first to do so and fails to cite other papers that have investigated sensory modulation of the motor cortex (Stavinksy et al. 2017 Neuron, Pruszynski et al. 2011 Nature, Omrani et al. 2016 eLife). These studies should be mentioned in the Introduction to capture better the context around the present study. It would also be

beneficial to add a discussion of how the results compare to the findings from these other works.

This study also uses insights from single-unit analysis to inform mechanistic models of these population dynamics, which is a powerful approach, but is dependent on the validity of the single-cell analysis, which I have expanded on below.

I have clarified some of the areas that would benefit from further analysis below:

(1) Task:
The task is well designed, although it would have benefited from perhaps one more target speed (for each direction). One monkey appears to have experienced one more target speed than the others (seen in Figure 3C). It would have been nice to have this data for all monkeys.

(2) Single unit analyses:
In some analyses, the effects of target speed look more driven by target movement direction (e.g. Figures 1D and E). To confirm target speed is the main modulator, it would be good to compare how much more variance is explained by models including speed rather than just direction. More target speeds may have been helpful here too.

The choice of the three categories (PD shift, gain addition) is not completely justified in a satisfactory way. It would be nice to see whether these three main categories are confirmed by unsupervised methods.

The decoder analyses in Figure 2 provide evidence that target speed modulation may change over the trial. Therefore, it is important to see how the window considered for the firing rate in Figure 1 (currently 100ms pre - 100ms post movement onset) affects the results.

(3) Decoder:
One feature of the task is that the reach endpoints tile the entire perimeter of the target circle (Figure 1B). However, this feature is not exploited for much of the single-unit analyses. This is most notable in Figure 2, where the use of a SVM limits the decoding to discrete values (the endpoints are divided into 8 categories). Using continuous decoding of hand kinematics would be more appropriate for this task.

(4) RNN:
Mixed selectivity is not analysed in the RNN, which would help to compare the model to the real data where mixed selectivity is common. Furthermore, it would be informative to compare the neural data to the RNN activity using canonical correlation or Procrustes analyses. These would help validate the claim of similarity between RNN and neural dynamics, rather than allowing comparisons to be dominated by geometric similarities that may be features of the task. There is also an absence of alternate models to compare the perturbation model results to.

https://doi.org/10.7554/eLife.100064.1.sa3

Reviewer #2 (Public Review):

Summary:

In this manuscript, Zhang et al. examine neural activity in the motor cortex as monkeys make reaches in a novel target interception task. Zhang et al. begin by examining the single neuron tuning properties across different moving target conditions, finding several classes of neurons: those that shift their preferred direction, those that change their modulation gain, and those that shift their baseline firing rates. The authors go on to find an interesting, tilted ring structure of the neural population activity, depending on the target speed, and find that

(1) the reach direction has consistent positioning around the ring, and (2) the tilt of the ring is highly predictive of the target movement speed. The authors then model the neural activity with a single neuron representational model and a recurrent neural network model, concluding that this population structure requires a mixture of the three types of single neurons described at the beginning of the manuscript.

Strengths:

I find the task the authors present here to be novel and exciting. It slots nicely into an overall trend to break away from a simple reach-to-static-target task to better characterize the breadth of how the motor cortex generates movements. I also appreciate the movement from single neuron characterization to population activity exploration, which generally serves to anchor the results and make them concrete. Further, the orbital ring structure of population activity is fascinating, and the modeling work at the end serves as a useful baseline control to see how it might arise.

Weaknesses:

While I find the behavioral task presented here to be excitingly novel, I find the presented analyses and results to be far less interesting than they could be. Key to this, I think, is that the authors are examining this task and related neural activity primarily with a single-neuron representational lens. This would be fine as an initial analysis since the population activity is of course composed of individual neurons, but the field seems to have largely moved towards a more abstract "computation through dynamics" framework that has, in the last several years, provided much more understanding of motor control than the representational framework has. As the manuscript stands now, I'm not entirely sure what interpretation to take away from the representational conclusions the authors made (i.e. the fact that the orbital population geometry arises from a mixture of different tuning types). As such, by the end of the manuscript, I'm not sure I understand any better how the motor cortex or its neural geometry might be contributing to the execution of this novel task.

Main Comments:

My main suggestions to the authors revolve around bringing in the computation through a dynamics framework to strengthen their population results. The authors cite the Vyas et al. review paper on the subject, so I believe they are aware of this framework. I have three suggestions for improving or adding to the population results:

(1) Examination of delay period activity: one of the most interesting aspects of the task was the fact that the monkey had a random-length delay period before he could move to intercept the target. Presumably, the monkey had to prepare to intercept at any time between 400 and 800 ms, which means that there may be some interesting preparatory activity dynamics during this period. For example, after 400ms, does the preparatory activity rotate with the target such that once the go cue happens, the correct interception can be executed? There is some analysis of the delay period population activity in the supplement, but it doesn't quite get at the question of how the interception movement is prepared. This is perhaps the most interesting question that can be asked with this experiment, and it's one that I think may be quite novel for the field--it is a shame that it isn't discussed.

(2) Supervised examination of population structure via potent and null spaces: simply examining the first three principal components revealed an orbital structure, with a seemingly conserved motor output space and a dimension orthogonal to it that relates to the visual input. However, the authors don't push this insight any further. One way to do that would be to find the "potent space" of motor cortical activity by regression to the arm movement and examine how the tilted rings look in that space (this is actually fairly easy to see in the reach direction components of the dPCA plot in the supplement--the rings will be highly aligned in this space). Presumably, then, the null space should contain information

about the target movement. dPCA shows that there's not a single dimension that clearly delineates target speed, but the ring tilt is likely evident if the authors look at the highest variance neural dimension orthogonal to the potent space (the "null space")--this is akin to PC3 in the current figures, but it would be nice to see what comes out when you look in the data for it.

(3) RNN perturbations: as it's currently written, the RNN modeling has promise, but the perturbations performed don't provide me with much insight. I think this is because the authors are trying to use the RNN to interpret the single neuron tuning, but it's unclear to me what was learned from perturbing the connectivity between what seems to me almost arbitrary groups of neurons (especially considering that 43% of nodes were unclassifiable). It seems to me that a better perturbation might be to move the neural state before the movement onset to see how it changes the output. For example, the authors could move the neural state from one tilted ring to another to see if the virtual hand then reaches a completely different (yet predictable) target. Moreover, if the authors can more clearly characterize the preparatory movement, perhaps perturbations in the delay period would provide even more insight into how the interception might be prepared.

https://doi.org/10.7554/eLife.100064.1.sa2

Reviewer #3 (Public Review):

Summary:

This experimental study investigates the influence of sensory information on neural population activity in M1 during a delayed reaching task. In the experiment, monkeys are trained to perform a delayed interception reach task, in which the goal is to intercept a potentially moving target.

This paradigm allows the authors to investigate how, given a fixed reach endpoint (which is assumed to correspond to a fixed motor output), the sensory information regarding the target motion is encoded in neural activity.

At the level of single neurons, the authors found that target motion modulates the activity in three main ways: gain modulation (scaling of the neural activity depending on the target direction), shift (shift of the preferred direction of neurons tuned to reach direction), or addition (offset to the neural activity).

At the level of the neural population, target motion information was largely encoded along the 3rd PC of the neural activity, leading to a tilt of the manifold along which reach direction was encoded that was proportional to the target speed. The tilt of the neural manifold was found to be largely driven by the variation of activity of the population of gain-modulated neurons.
Finally, the authors studied the behaviour of an RNN trained to generate the correct hand velocity given the sensory input and reach direction. The RNN units were found to similarly exhibit mixed selectivity to the sensory information, and the geometry of the « neural population » resembled that observed in the monkeys.

Strengths:

- The experiment is well set up to address the question of how sensory information that is directly relevant to the behaviour but does not lead to a direct change in behavioural output modulates motor cortical activity.

- The finding that sensory information modulates the neural activity in M1 during motor preparation and execution is non trivial, given that this modulation of the activity must occur

in the nullspace of the movement.

- The paper gives a complete picture of the effect of the target motion on neural activity, by including analyses at the single neuron level as well as at the population level. Additionally, the authors link those two levels of representation by highlighting how gain modulation contributes to shaping the population representation.

Weaknesses:

- One of the main premises of the paper is the fact that the motor output for a given reach point is preserved across different target motions. However, as the authors briefly mention in the conclusion, they did not record muscle activity during the task, but only hand velocity, making it impossible to directly verify how preserved muscle patterns were across movements. While the authors highlight that they did not see any difference in their results when resampling the data to control for similar hand velocities across conditions, this seems like an important potential caveat of the paper whose implications should be discussed further or highlighted earlier in the paper.

- The main takeaway of the RNN analysis is not fully clear. The authors find that an RNN trained given a sensory input representing a moving target displays modulation to target motion that resembles what is seen in real data. This is interesting, but the authors do not dissect why this representation arises, and how robust it is to various task design choices. For instance, it appears that the network should be able to solve the task using only the motion intention input, which contains the reach endpoint information. If the target motion input is not used for the task, it is not obvious why the RNN units would be modulated by this input (especially as this modulation must lie in the nullspace of the movement hand velocity if the velocity depends only on the reach endpoint). It would thus be important to see alternative models compared to true neural activity, in addition to the model currently included in the paper. Besides, for the model in the paper, it would therefore be interesting to study further how the details of the network setup (eg initial spectral radius of the connectivity, weight regularization, or using only the target position input) affect the modulation by the motion input, as well as the trained population geometry and the relative ratios of modulated cells after training.

- Additionally, it is unclear what insights are gained from the perturbations to the network connectivity the authors perform, as it is generally expected that modulating the connectivity will degrade task performance and the geometry of the responses. If the authors wish the make claims about the role of the subpopulations, it could be interesting to test whether similar connectivity patterns develop in networks that are not initialized with an all-to-all random connectivity or to use ablation experiments to investigate whether the presence of multiple types of modulations confers any sort of robustness to the network.

- The results suggest that the observed changes in motor cortical activity with target velocity result from M1 activity receiving an input that encodes the velocity information. This also appears to be the assumption in the RNN model. However, even though the input shown to the animal during preparation is indeed a continuously moving target, it appears that the only relevant quantity to the actual movement is the final endpoint of the reach. While this would have to be a function of the target velocity, one could imagine that the computation of where the monkeys should reach might be performed upstream of the motor cortex, in which case the actual target velocity would become irrelevant to the final motor output. This makes the results of the paper very interesting, but it would be nice if the authors could discuss further when one might expect to see modulation by sensory information that does not directly affect motor output in M1, and where those inputs may come from. It may also be interesting to discuss how the findings relate to previous work that has found behaviourally irrelevant information is being filtered out from M1 (for instance, Russo et al, Neuron 2020 found that in monkeys performing a cycling task, context can be decoded from SMA but not

from M1, and Wang et al, Nature Communications 2019 found that perceptual information could not be decoded from PMd)?

https://doi.org/10.7554/eLife.100064.1.sa1

Author response:

> ***eLife assessment***
>
> *This useful study examines the neural activity in the motor cortex as a monkey reaches to intercept moving targets, focusing on how tuned single neurons contribute to an interesting overall population geometry. The presented results and analyses are solid, though the investigation of this novel task could be strengthened by clarifying the assumptions behind the single neuron analyses, and further analyses of the neural population activity and its relation to different features of behaviour.*

Thanks for recognizing the content of our research, and please stay tuned for our follow-up studies on neural dynamics during interception.

> ***Public Reviews:***
>
> ***Reviewer #1 (Public Review):***
>
> *Summary:*
>
> *This study addresses the question of how task-relevant sensory information affects activity in the motor cortex. The authors use various approaches to address this question, looking at single units and population activity. They find that there are three subtypes of modulation by sensory information at the single unit level. Population analyses reveal that sensory information affects the neural activity orthogonally to motor output. The authors then compare both single unit and population activity to computational models to investigate how encoding of sensory information at the single unit level is coordinated in a network. They find that an RNN that displays similar orbital dynamics and sensory modulation to the motor cortex also contains nodes that are modulated similarly to the three subtypes identified by the single unit analysis.*
>
> *Strengths:*
>
> *The strengths of this study lie in the population analyses and the approach of comparing single-unit encoding to population dynamics. In particular, the analysis in Figure 3 is very elegant and informative about the effect of sensory information on motor cortical activity. The task is also well designed to suit the questions being asked and well controlled.*

We appreciate these kind comments.

> *It is commendable that the authors compare single units to population modulation. The addition of the RNN model and perturbations strengthen the conclusion that the subtypes of individual units all contribute to the population dynamics. However, the subtypes (PD shift, gain, and addition) are not sufficiently justified. The authors also do not address that single units exhibit mixed modulation, but RNN units are not treated as such.*

We're sorry for not providing sufficient grounds to introduce the subtypes. We determined the PD shift, gain, and addition as pertinent subtypes based on classical cosine tuning model

(Georgopoulos et al., 1982) and referred to some gain modulation studies (e.g. Pesaran et al. 2010, Bremner and Andersen, 2012). Here, we applied this subtype analysis as a criteria to identify the modulation in neuronal population rather than to sort neuron into distinct cell types. We will update Methods in the revised version of manuscript.

> *Weaknesses:*
>
> *The main weaknesses of the study lie in the categorization of the single units into PD shift, gain, and addition types. The single units exhibit clear mixed selectivity, as the authors highlight. Therefore, the subsequent analyses looking only at the individual classes in the RNN are a little limited. Another weakness of the paper is that the choice of windows for analyses is not properly justified and the dependence of the results on the time windows chosen for single-unit analyses is not assessed. This is particularly pertinent because tuning curves are known to rotate during movements (Sergio et al. 2005 Journal of Neurophysiology).*

The mixed selectivity or precisely the mixed modulation is indeed a significant feature of neuronal population in the present study. The purpose of the subtype analysis was to serve as a criterion for the potential modulation mechanisms. However, the results appear to be a spectrum than clusters. It still through some insights to understand the modulation distribution and we will refine the description in the next version. In the current version, we observed single-unit tuning and population neural state with sliding windows, focusing on the period around movement onset (MO) due to the emergence of a ring-like structure. We will clarify the choice of windows and the dependence assessment in the next version. It's a great suggestion to consider the role of rotating tuning curves in neural dynamics during interception.

> *This paper shows sensory information can affect motor cortical activity whilst not affecting motor output. However, it is not the first to do so and fails to cite other papers that have investigated sensory modulation of the motor cortex (Stavinksy et al. 2017 Neuron, Pruszynski et al. 2011 Nature, Omrani et al. 2016 eLife). These studies should be mentioned in the Introduction to capture better the context around the present study. It would also be beneficial to add a discussion of how the results compare to the findings from these other works.*

Thanks for the reminder. We will introduce the relevant research in the next version of manuscript.

> *This study also uses insights from single-unit analysis to inform mechanistic models of these population dynamics, which is a powerful approach, but is dependent on the validity of the single-cell analysis, which I have expanded on below.*
>
> *I have clarified some of the areas that would benefit from further analysis below:*
>
> *(1) Task:*
>
> *The task is well designed, although it would have benefited from perhaps one more target speed (for each direction). One monkey appears to have experienced one more target speed than the others (seen in Figure 3C). It would have been nice to have this data for all monkeys.*

Great suggestion! However, it's hard to implement as the implanted arrays have been removed.

> *(2) Single unit analyses:*

> *In some analyses, the effects of target speed look more driven by target movement direction (e.g. Figures 1D and E). To confirm target speed is the main modulator, it would be good to compare how much more variance is explained by models including speed rather than just direction. More target speeds may have been helpful here too.*

Nice suggestion! The fitting goodness of the simple model (just motor direction) is much less than the complex model (including target speed). We will update the results in the next version.

> *The choice of the three categories (PD shift, gain addition) is not completely justified in a satisfactory way. It would be nice to see whether these three main categories are confirmed by unsupervised methods.*

A good point. We will have a try with unsupervised methods.

> *The decoder analyses in Figure 2 provide evidence that target speed modulation may change over the trial. Therefore, it is important to see how the window considered for the firing rate in Figure 1 (currently 100ms pre - 100ms post movement onset) affects the results.*

Thanks for the suggestion and close reading. We will test the decoder in other epochs.

> *(3) Decoder:*
>
> *One feature of the task is that the reach endpoints tile the entire perimeter of the target circle (Figure 1B). However, this feature is not exploited for much of the single-unit analyses. This is most notable in Figure 2, where the use of a SVM limits the decoding to discrete values (the endpoints are divided into 8 categories). Using continuous decoding of hand kinematics would be more appropriate for this task.*

This is a very reasonable suggestion. In this study, we discrete the reach-direction as the previous studies (Li et al., 2018&2022) and thought that the discrete decoding was already enough to show the interaction of sensory and motor variables. In future studies, we will try continuous decoding of hand kinematics.

> *(4) RNN:*
>
> *Mixed selectivity is not analysed in the RNN, which would help to compare the model to the real data where mixed selectivity is common. Furthermore, it would be informative to compare the neural data to the RNN activity using canonical correlation or Procrustes analyses. These would help validate the claim of similarity between RNN and neural dynamics, rather than allowing comparisons to be dominated by geometric similarities that may be features of the task. There is also an absence of alternate models to compare the perturbation model results to.*

Thank you for these helpful suggestions. We will perform decoding analysis on RNN units to verify if there is interaction of sensory and motor variables as in real data, as well as the canonical correlation or Procrustes analysis.

> ***Reviewer #2 (Public Review):***
>
> *Summary:*
>
> *In this manuscript, Zhang et al. examine neural activity in the motor cortex as monkeys make reaches in a novel target interception task. Zhang et al. begin by examining the*

> *single neuron tuning properties across different moving target conditions, finding several classes of neurons: those that shift their preferred direction, those that change their modulation gain, and those that shift their baseline firing rates. The authors go on to find an interesting, tilted ring structure of the neural population activity, depending on the target speed, and find that (1) the reach direction has consistent positioning around the ring, and (2) the tilt of the ring is highly predictive of the target movement speed. The authors then model the neural activity with a single neuron representational model and a recurrent neural network model, concluding that this population structure requires a mixture of the three types of single neurons described at the beginning of the manuscript.*
>
> *Strengths:*
>
> *I find the task the authors present here to be novel and exciting. It slots nicely into an overall trend to break away from a simple reach-to-static-target task to better characterize the breadth of how the motor cortex generates movements. I also appreciate the movement from single neuron characterization to population activity exploration, which generally serves to anchor the results and make them concrete. Further, the orbital ring structure of population activity is fascinating, and the modeling work at the end serves as a useful baseline control to see how it might arise.*

Thank you for recognizing our work.

> *Weaknesses:*
>
> *While I find the behavioral task presented here to be excitingly novel, I find the presented analyses and results to be far less interesting than they could be. Key to this, I think, is that the authors are examining this task and related neural activity primarily with a single-neuron representational lens. This would be fine as an initial analysis since the population activity is of course composed of individual neurons, but the field seems to have largely moved towards a more abstract "computation through dynamics" framework that has, in the last several years, provided much more understanding of motor control than the representational framework has. As the manuscript stands now, I'm not entirely sure what interpretation to take away from the representational conclusions the authors made (i.e. the fact that the orbital population geometry arises from a mixture of different tuning types). As such, by the end of the manuscript, I'm not sure I understand any better how the motor cortex or its neural geometry might be contributing to the execution of this novel task.*

The present study shows the sensory modulation on motor tuning in single units and neural state during motor execution period. It's a pity that the findings were constrained in certain time windows. We are still working this topic, and hopefully will address related questions in our follow-up studies.

> *Main Comments:*
>
> *My main suggestions to the authors revolve around bringing in the computation through a dynamics framework to strengthen their population results. The authors cite the Vyas et al. review paper on the subject, so I believe they are aware of this framework. I have three suggestions for improving or adding to the population results:*
>
> *(1) Examination of delay period activity: one of the most interesting aspects of the task was the fact that the monkey had a random-length delay period before he could move to intercept the target. Presumably, the monkey had to prepare to intercept at any time between 400 and 800 ms, which means that there may be some interesting preparatory activity dynamics during this period. For example, after 400ms, does the preparatory*

> *activity rotate with the target such that once the go cue happens, the correct interception can be executed? There is some analysis of the delay period population activity in the supplement, but it doesn't quite get at the question of how the interception movement is prepared. This is perhaps the most interesting question that can be asked with this experiment, and it's one that I think may be quite novel for the field--it is a shame that it isn't discussed.*

Great idea! We are on the way, and close to complete the puzzle.

> *(2) Supervised examination of population structure via potent and null spaces: simply examining the first three principal components revealed an orbital structure, with a seemingly conserved motor output space and a dimension orthogonal to it that relates to the visual input. However, the authors don't push this insight any further. One way to do that would be to find the "potent space" of motor cortical activity by regression to the arm movement and examine how the tilted rings look in that space (this is actually fairly easy to see in the reach direction components of the dPCA plot in the supplement--the rings will be highly aligned in this space). Presumably, then, the null space should contain information about the target movement. dPCA shows that there's not a single dimension that clearly delineates target speed, but the ring tilt is likely evident if the authors look at the highest variance neural dimension orthogonal to the potent space (the "null space")--this is akin to PC3 in the current figures, but it would be nice to see what comes out when you look in the data for it.*

Nice suggestion. Target-speed modulation mainly influences PC3, which is consistent with 'null space' hypothesis. We will try other methods of dimensionality reduction (e.g. dPCA, Manopt) to determine the potent and null space.

> *(3) RNN perturbations: as it's currently written, the RNN modeling has promise, but the perturbations performed don't provide me with much insight. I think this is because the authors are trying to use the RNN to interpret the single neuron tuning, but it's unclear to me what was learned from perturbing the connectivity between what seems to me almost arbitrary groups of neurons (especially considering that 43% of nodes were unclassifiable). It seems to me that a better perturbation might be to move the neural state before the movement onset to see how it changes the output. For example, the authors could move the neural state from one tilted ring to another to see if the virtual hand then reaches a completely different (yet predictable) target. Moreover, if the authors can more clearly characterize the preparatory movement, perhaps perturbations in the delay period would provide even more insight into how the interception might be prepared.*

We are sorry that we didn't clarify the definition of "none" type, which can be misleading. The 43% unclassified nodes include those inactive ones, when only activate (task-related) nodes included, the ratio of unclassified nodes would be much lower. By perturbing the connectivity, we intended to explore the interaction between different modulations.

Thank you for the great advice. We tried moving neural states from one ring to another without changing the directional cluster, but this perturbation didn't have a significant influence on network performance as expected. We will check this result again and try perturbations in the delay period.

> ***Reviewer #3 (Public Review):***
>
> *Summary:*

> *This experimental study investigates the influence of sensory information on neural population activity in M1 during a delayed reaching task. In the experiment, monkeys are trained to perform a delayed interception reach task, in which the goal is to intercept a potentially moving target.*
>
> *This paradigm allows the authors to investigate how, given a fixed reach endpoint (which is assumed to correspond to a fixed motor output), the sensory information regarding the target motion is encoded in neural activity.*
>
> *At the level of single neurons, the authors found that target motion modulates the activity in three main ways: gain modulation (scaling of the neural activity depending on the target direction), shift (shift of the preferred direction of neurons tuned to reach direction), or addition (offset to the neural activity).*
>
> *At the level of the neural population, target motion information was largely encoded along the 3rd PC of the neural activity, leading to a tilt of the manifold along which reach direction was encoded that was proportional to the target speed. The tilt of the neural manifold was found to be largely driven by the variation of activity of the population of gain-modulated neurons.*
>
> *Finally, the authors studied the behaviour of an RNN trained to generate the correct hand velocity given the sensory input and reach direction. The RNN units were found to similarly exhibit mixed selectivity to the sensory information, and the geometry of the « neural population » resembled that observed in the monkeys.*
>
> *Strengths:*
>
> *- The experiment is well set up to address the question of how sensory information that is directly relevant to the behaviour but does not lead to a direct change in behavioural output modulates motor cortical activity.*
>
> *- The finding that sensory information modulates the neural activity in M1 during motor preparation and execution is non trivial, given that this modulation of the activity must occur in the nullspace of the movement.*
>
> *- The paper gives a complete picture of the effect of the target motion on neural activity, by including analyses at the single neuron level as well as at the population level. Additionally, the authors link those two levels of representation by highlighting how gain modulation contributes to shaping the population representation.*

Thanks for your recognition.

> *Weaknesses:*
>
> *- One of the main premises of the paper is the fact that the motor output for a given reach point is preserved across different target motions. However, as the authors briefly mention in the conclusion, they did not record muscle activity during the task, but only hand velocity, making it impossible to directly verify how preserved muscle patterns were across movements. While the authors highlight that they did not see any difference in their results when resampling the data to control for similar hand velocities across conditions, this seems like an important potential caveat of the paper whose implications should be discussed further or highlighted earlier in the paper.*

Thanks for the suggestion. We will highlight the resampling results as important control in the next version of manuscript.

> *- The main takeaway of the RNN analysis is not fully clear. The authors find that an RNN trained given a sensory input representing a moving target displays modulation to target motion that resembles what is seen in real data. This is interesting, but the authors do not dissect why this representation arises, and how robust it is to various task design choices. For instance, it appears that the network should be able to solve the task using only the motion intention input, which contains the reach endpoint information. If the target motion input is not used for the task, it is not obvious why the RNN units would be modulated by this input (especially as this modulation must lie in the nullspace of the movement hand velocity if the velocity depends only on the reach endpoint). It would thus be important to see alternative models compared to true neural activity, in addition to the model currently included in the paper. Besides, for the model in the paper, it would therefore be interesting to study further how the details of the network setup (eg initial spectral radius of the connectivity, weight regularization, or using only the target position input) affect the modulation by the motion input, as well as the trained population geometry and the relative ratios of modulated cells after training.*

Great suggestions. It's a considerable pity that we didn't dissect the formation reason and influence factor of the representation in the current version. We've tried several combinations of inputs before: in the network which received only motor intention and GO inputs, there were rings but not tilting related to target-speed; in the network which received only target location and GO inputs, there were ring-like structures but not clear directional clusters. We will check these results and try alternative models in the next version. In future studies, we will examine the influence of network setup details.

> *- Additionally, it is unclear what insights are gained from the perturbations to the network connectivity the authors perform, as it is generally expected that modulating the connectivity will degrade task performance and the geometry of the responses. If the authors wish the make claims about the role of the subpopulations, it could be interesting to test whether similar connectivity patterns develop in networks that are not initialized with an all-to-all random connectivity or to use ablation experiments to investigate whether the presence of multiple types of modulations confers any sort of robustness to the network.*

Thank you for the great suggestions. By perturbations, we intended to explore the contribution of interaction between certain subpopulations. We tried ablation experiments, but the result was not significant. Probably because the most units were of mixed selectivity, the units of only modulations were not enough for bootstrapping, or the random sampling from single subpopulation (bearing mixed selectivity) could be repeated. We will consider these suggestions carefully in the revised version.

> *- The results suggest that the observed changes in motor cortical activity with target velocity result from M1 activity receiving an input that encodes the velocity information. This also appears to be the assumption in the RNN model. However, even though the input shown to the animal during preparation is indeed a continuously moving target, it appears that the only relevant quantity to the actual movement is the final endpoint of the reach. While this would have to be a function of the target velocity, one could imagine that the computation of where the monkeys should reach might be performed upstream of the motor cortex, in which case the actual target velocity would become irrelevant to the final motor output. This makes the results of the paper very interesting, but it would be nice if the authors could discuss further when one might expect to see modulation by sensory information that does not directly affect motor output in M1, and where those inputs may come from. It may also be interesting to discuss how the findings relate to previous work that has found behaviourally irrelevant information is*

> *being filtered out from M1 (for instance, Russo et al, Neuron 2020 found that in monkeys performing a cycling task, context can be decoded from SMA but not from M1, and Wang et al, Nature Communications 2019 found that perceptual information could not be decoded from PMd)?*

How and where sensory information modulates M1 are very interesting and open questions. We will discuss further about this topic in the next version.

https://doi.org/10.7554/eLife.100064.1.sa0